Research Article

Design of a Multiband Antenna for LTE/GSM/UMTS Band Operation

Youngtaek Hong, Jinpil Tak, Jisoo Baek, Bongsik Myeong, and Jaehoon Choi

*Department of Electronics and Communications Engineering, Hanyang University, 222 Wangsimni-ro,
Seongdong-gu, Seoul 133-791, Republic of Korea*

Correspondence should be addressed to Jaehoon Choi; choijh@hanyang.ac.kr

This paper proposes a multiband antenna for LTE/GSM/UMTS band operation. The proposed antenna consists of a meandered planar inverted-F antenna with an additional branch line for wide bandwidth and a folded-loop antenna. The antenna provides a wide bandwidth to cover the hepta-band LTE/GSM/UMTS operation. The measured 6 dB return loss bandwidth is 169 MHz (793–962 MHz) at the low-frequency band and 1030 MHz (1700–2730 MHz) at the high-frequency band. The overall dimension of the proposed antenna is 55 mm × 110 mm × 5 mm.

1. Introduction

Nowadays, mobile equipment is required to cover various communication services (Wi-Fi, Bluetooth, GPS, and LTE). In various mobile communication services, long-term evolution (LTE) is one of the widely used communication systems as a fourth-generation wireless service. Because each nation or wireless carrier uses different frequency bands, a multiband antenna is desirable. Moreover, the role of multiband antennas becomes more important because the carrier aggregation technique of LTE-Advanced communication system has been released [1].

In this paper, we propose a multiband antenna that operates over the hepta-band in LTE/GSM/UMTS services. The proposed antenna consists of a folded-loop and a meandered planar inverted-F antenna (MPIFA) with an additional branch line. The folded-loop antenna operates at the high-frequency band covering GSM1800 (1710–1880 MHz), GSM1900 (1850–1990 MHz), UMTS (1920–2170 MHz), LTE2300 (2305–2400 MHz), and LTE2500 (2500–2690 MHz), and the MPIFA with an additional branch line covers the low-frequency band, including GSM850 (824–894 MHz) and GSM900 (880–960 MHz) [2–6]. The proposed antenna satisfies the 6 dB return loss

bandwidth in all operating frequency bands and exhibits near-omnidirectional radiation patterns.

2. Antenna Design

Figure 1(a) shows the structure of the proposed multiband antenna for LTE/GSM/UMTS operation. The proposed antenna is designed on an FR-4 substrate (ε_r = 4.4; tanδ = 0.02). The FR-4 substrate dimension is 55 mm × 110 mm × 1 mm, and that of the antenna is 55 mm × 12 mm × 4 mm. Figure 1(b) shows the detailed configuration of the radiating element. The left side structure operates as a folded loop for the high-frequency band. This folded-loop structure has a wide bandwidth characteristic owing to its large thickness of 4 mm [7–9], whereas the right side structure that consists of an MPIFA and additional branch line covers the low-frequency band. Because a conventional PIFA has an insufficient frequency bandwidth for wireless communication, the proposed MPIFA has an additional branch line to increase the bandwidth. This structure generates additional resonance owing to the shunt capacitance between the additional branch line and the ground [10]. We used the HFSS v.14.0.0 by ANSYS for the simulation of the proposed antenna [11].
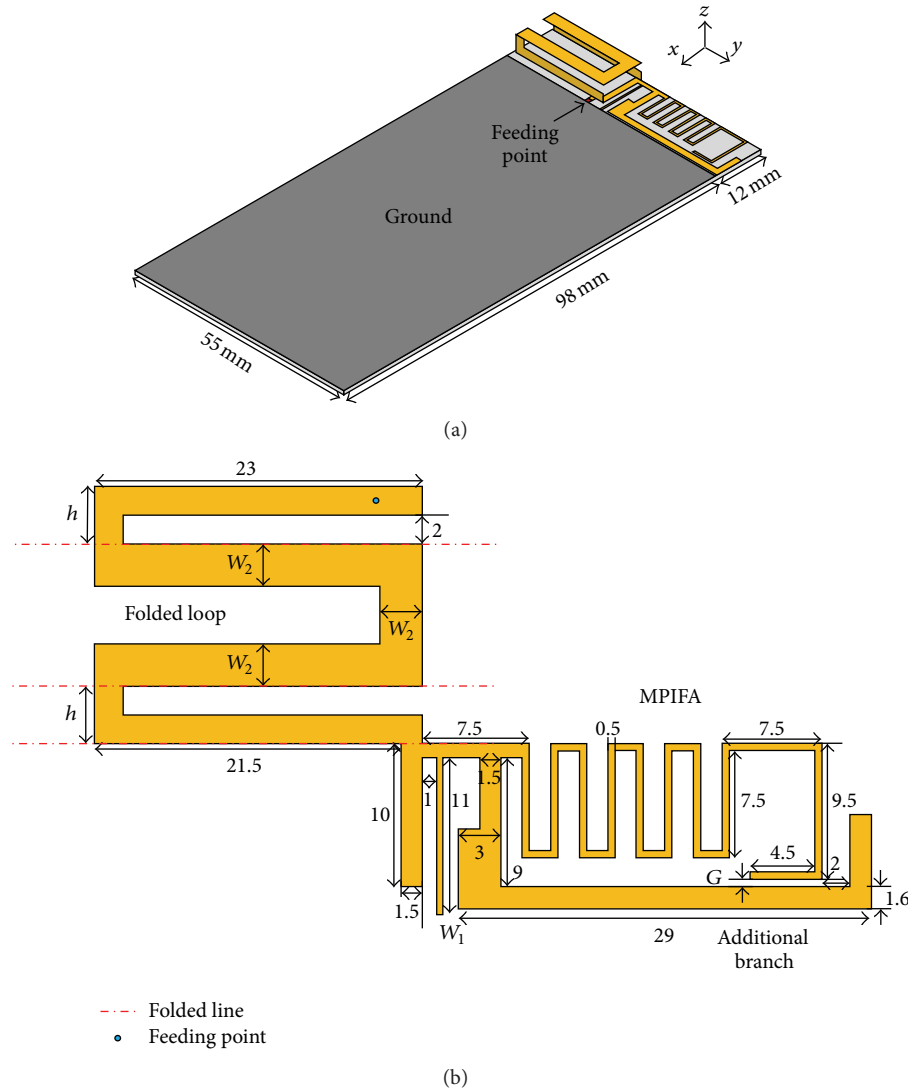
FIGURE 1: Configuration of the proposed antenna. (a) Overview. (b) Radiator.

3. Design Procedure and Parametric Study

To demonstrate the operating principle of the proposed antenna, it is divided into a folded-loop and an MPIFA structure. Figure 2 shows the simulated return loss characteristics of two reference antennas (Refs. 1 and 2) and the proposed antenna. The single element of the folded-loop antenna (Ref. 1) has a wide return loss bandwidth characteristic at the high-frequency band, whereas the single element of the MPIFA (Ref. 2) has narrow bandwidths at both the low and high bands. The Ref. 2 antenna without an additional branch line generates the first resonance at around 850 MHz and the second resonance at 2.5 GHz. By combining the folded-loop structure and the MPIFA with an additional branch line, the proposed antenna enhances the resonance characteristic at the high-frequency band and has a wide bandwidth characteristic at both low and high bands.

Parametric studies and optimization are performed for impedance matching at each resonant frequency and for determining the resonant frequency. Figure 3 shows the simulated return loss characteristics of various shorted strip widths W_1 of the MPIFA. As W_1 decreases, the second resonant frequency at the low band shifts to the lower frequency side, and impedance matching in the low-frequency band improves. However, the high-frequency band is not affected.

For overall impedance matching at the high-frequency band, the effect of height h of the folded-loop structure is shown in Figure 4. The return loss characteristic at the high-frequency band is improved by increasing h, whereas the first and second resonances at the low band remain almost stationary at around 800–1000 MHz. When $h = 4$ mm, the 6 dB return loss bandwidth at the high-frequency band simultaneously satisfies the GSM, UMTS, and LTE bands.

Figure 5 shows the simulated return loss characteristic for various widths of the folded loop W_2. As W_2 is increased, the effective current path of the folded loop structure is shortened so that the second resonance in the high-frequency band shifts toward the higher frequency side. Therefore the overall
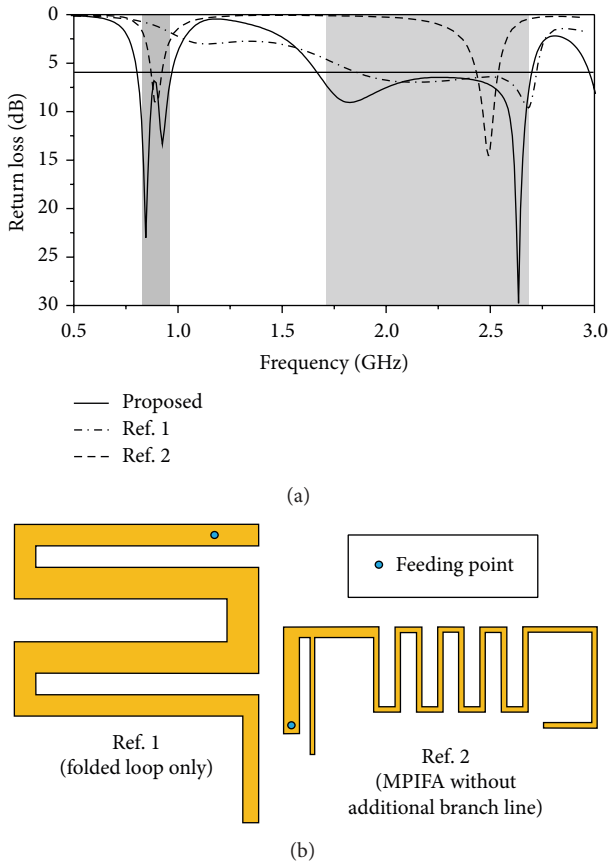
(a)

(b)

Figure 2: Simulated return loss characteristics of the proposed antenna for the folded-loop only case (Ref. 1) and for MPIFA without an additional branch line (Ref. 2) case. The dimensions of these reference antennas are shown in Figure 1.
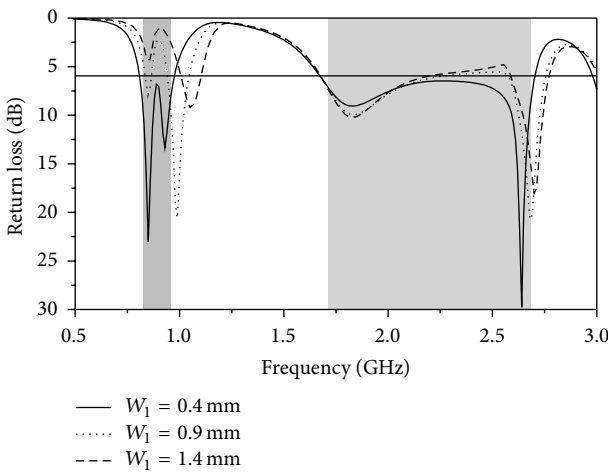

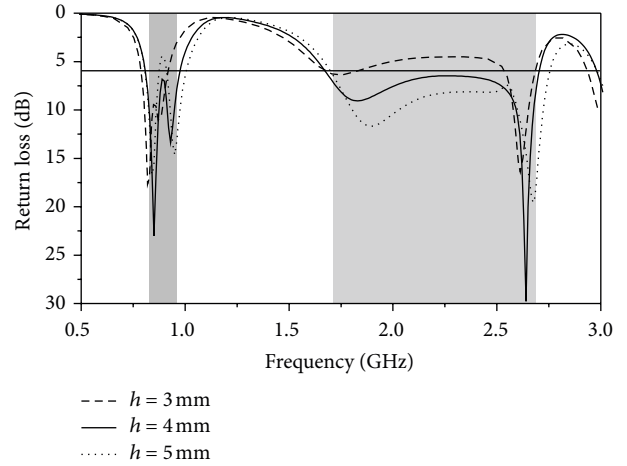Figure 3: Return loss characteristics of the various shorted strip widths of MPIFA.

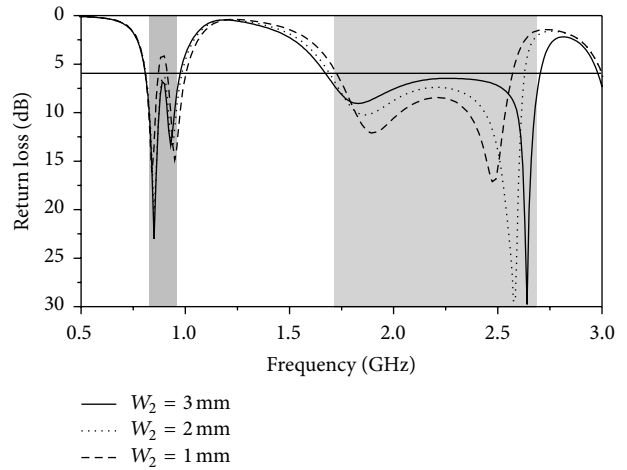Figure 4: Return loss characteristics for various heights of the folded-loop structure.

Figure 5: Return loss characteristics for various widths of the folded-loop structure.
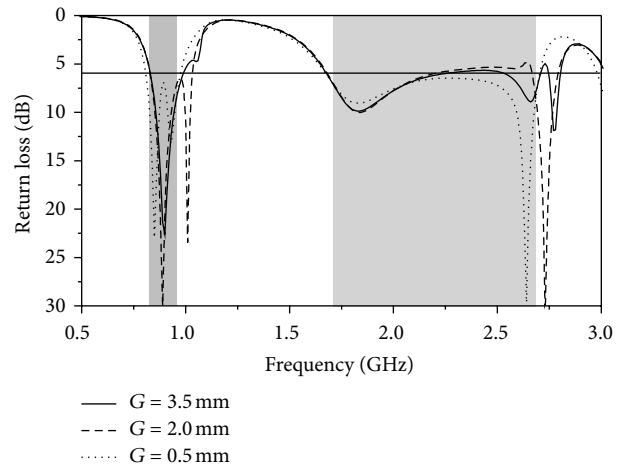
Figure 6: Return loss characteristics for various gap distances.

bandwidth at the high-frequency band is widened. When W_2 = 3 mm, the antenna satisfies the 6 dB return loss bandwidth at the desired frequency band.

Figure 6 shows the simulated return loss characteristic for various gap distance G. As G is decreased, the additional branch line is coupled strongly with MPIFA. Hence, the
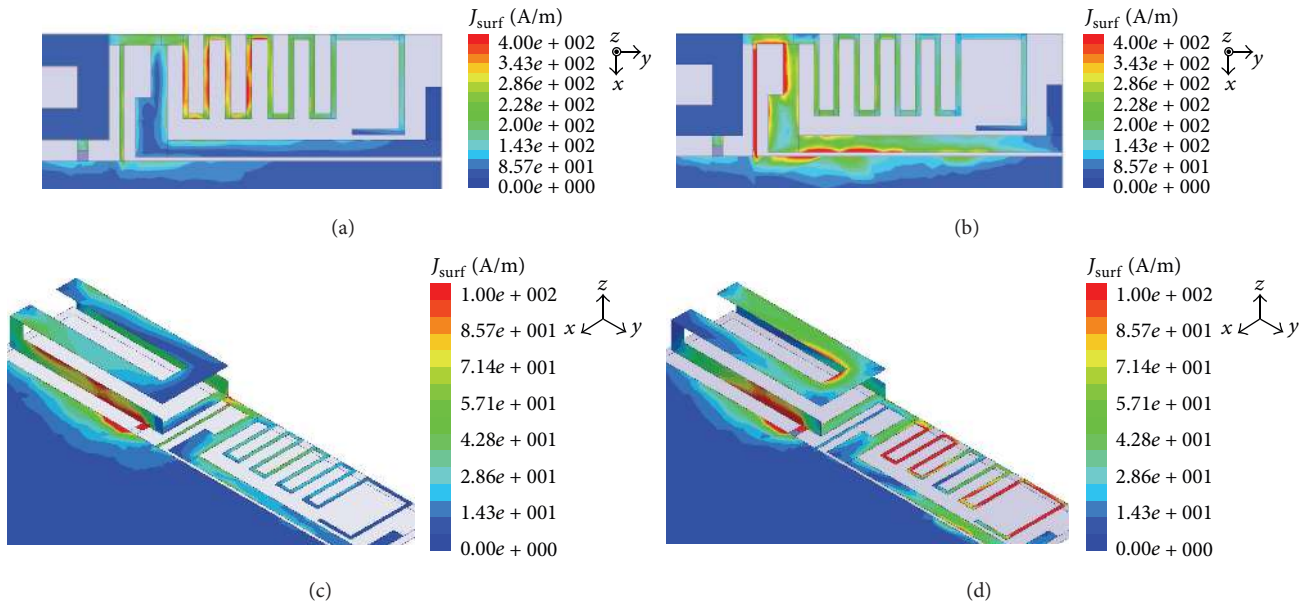
(a)

(b)

(c)

(d)

FIGURE 7: Simulated surface current distributions of the proposed antenna. (a) First resonance at low band (850 MHz). (b) Second resonance at low band (930 MHz). (c) First resonance at high band (1810 MHz). (d) Second resonance at high band (2640 MHz).
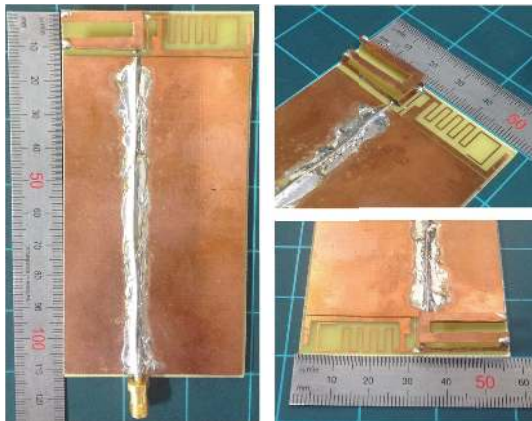

FIGURE 8: Photographs of the manufactured antenna.

FIGURE 9: Simulated and measured return loss characteristics of the proposed antenna.

effective length of additional branch line becomes larger and the second resonance in the low-frequency band shifts toward the low-frequency side. When $G = 0.5$ mm, the antenna has a dual resonance characteristic in the low-frequency band and the antenna satisfies 6 dB return loss bandwidth over the GSM 850 and GSM 900 bands. As a result, the simulated 6 dB return loss bandwidth of the proposed antenna is 166 MHz (809–975 MHz) at the low-frequency band and 1028 MHz (1675–2703 MHz) at the high-frequency band.

4. Results and Discussion

Figures 7(a) and 7(b) show the simulated surface current distributions of the MPIFA with a branch line at each resonant frequency at the low band (850 and 930 MHz). Two different current paths exist in this structure: one flows through the MPIFA; the other is formed by the coupling
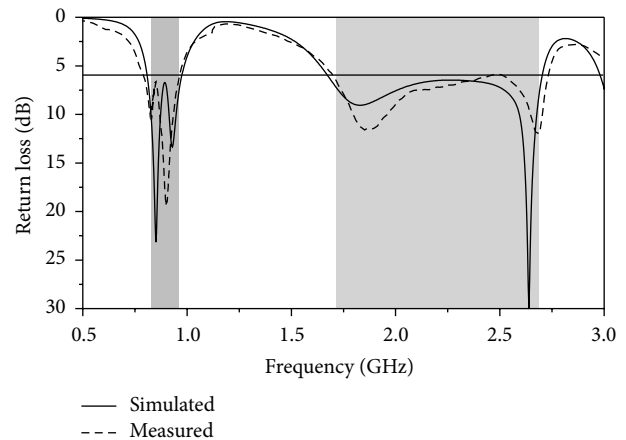
between the branch line and ground. At the resonance generated by the branch line, the radiation efficiency is bad because of the strong coupling. To improve the radiation characteristic in this case, a parasitic stub is added at the end of the additional branch line. Figures 7(a)–7(c) show that each structure, respectively, operates independently at its own resonance frequency. However, at the highest operating frequency, the current is strongly distributed in both the folded loop and MPIFA, as shown in Figure 7(d).

Figure 8 shows the photographs of the fabricated antenna. In the experiment, a 50-Ω coaxial line is used to feed the antenna.

Figure 9 shows the simulated and measured return loss characteristics of the proposed antenna. The measured results agree well with the simulated results. The measured 6 dB return loss bandwidths are 169 MHz (793–962 MHz) at the
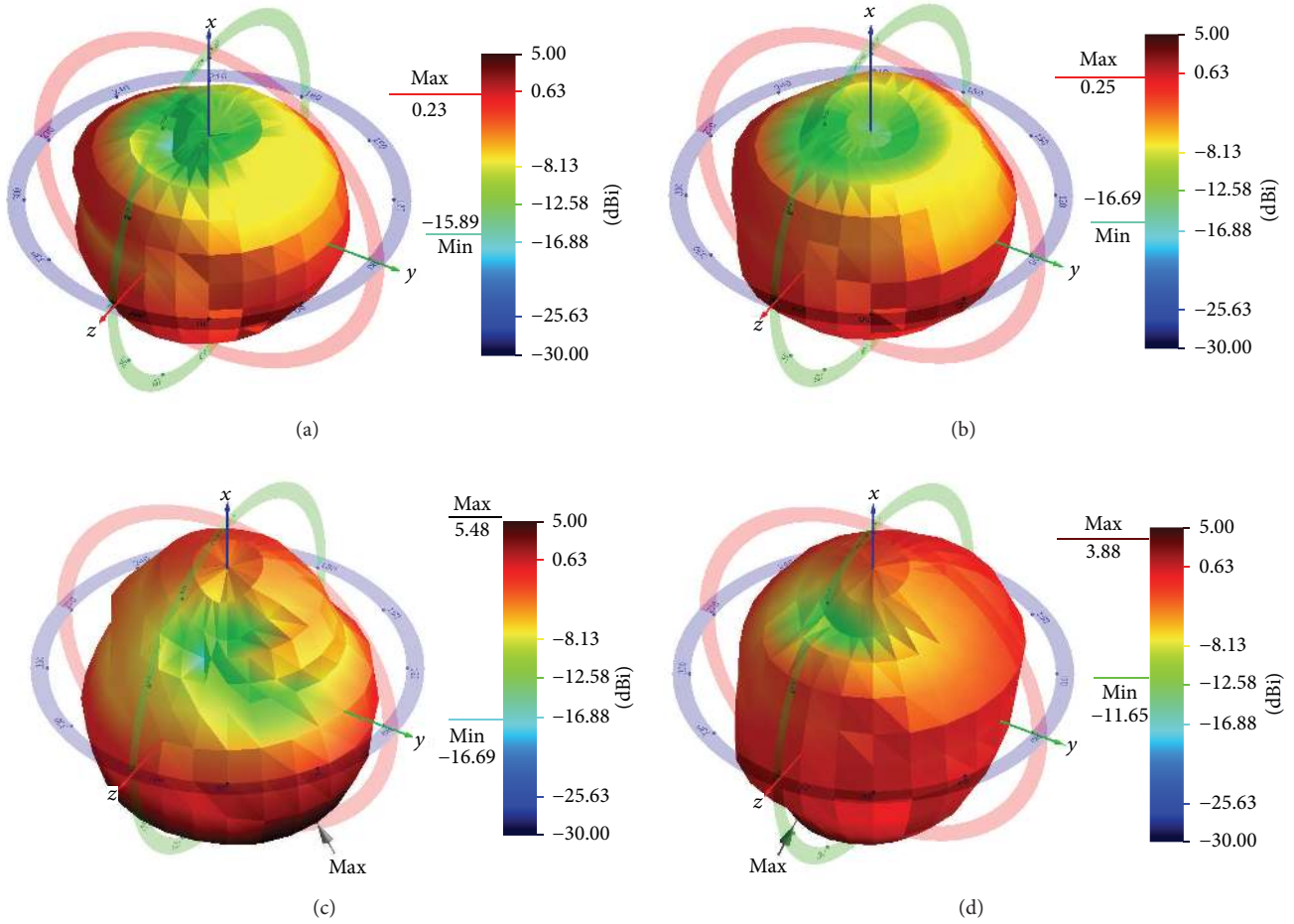
Figure 10: Measured 3D radiation patterns of the fabricated antenna at (a) 828 MHz, (b) 902 MHz, (c) 1850 MHz, and (d) 2680 MHz.
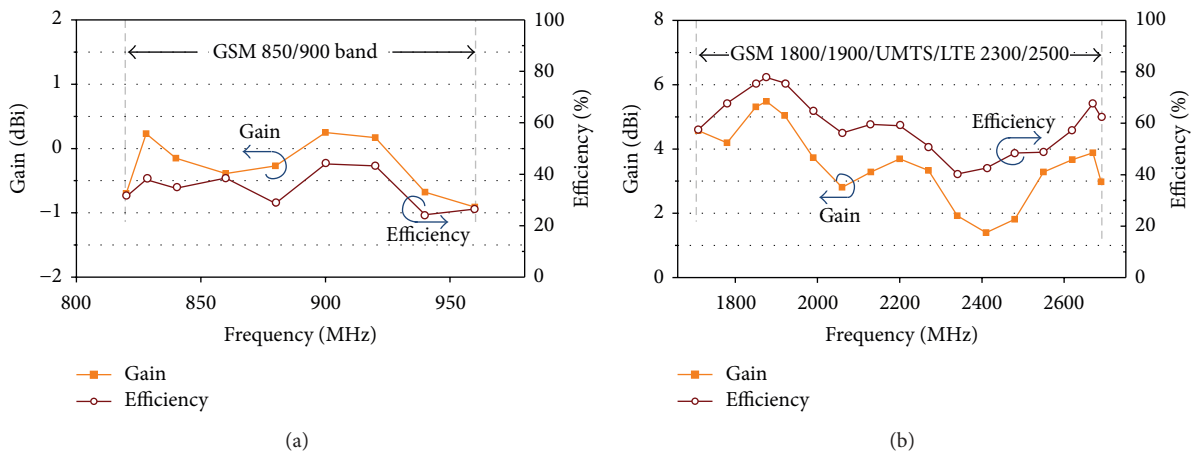

Figure 11: Measured antenna gain and radiation efficiency of the proposed antenna. (a) Low-frequency band. (b) High-frequency band.

low-frequency band and 1030 MHz (1700–2730 MHz) at the high-frequency band. This proposed antenna bandwidth is wide enough to cover the desired hepta-band.

Figure 10 shows the measured radiation patterns of the proposed antenna at each resonant frequency. At low frequencies of 828 and 902 MHz, the proposed antenna shows omnidirectional patterns. At high frequencies of 1850 and 2680 MHz, the proposed antenna shows directional patterns. The measured radiation patterns are suitable for practical mobile communication systems.

Figure 11 shows the measured radiation efficiency and measured gains of the proposed antenna. The measured radiation efficiency is approximately 24%–44% and 40%–78% at the low and high band, respectively. The radiation
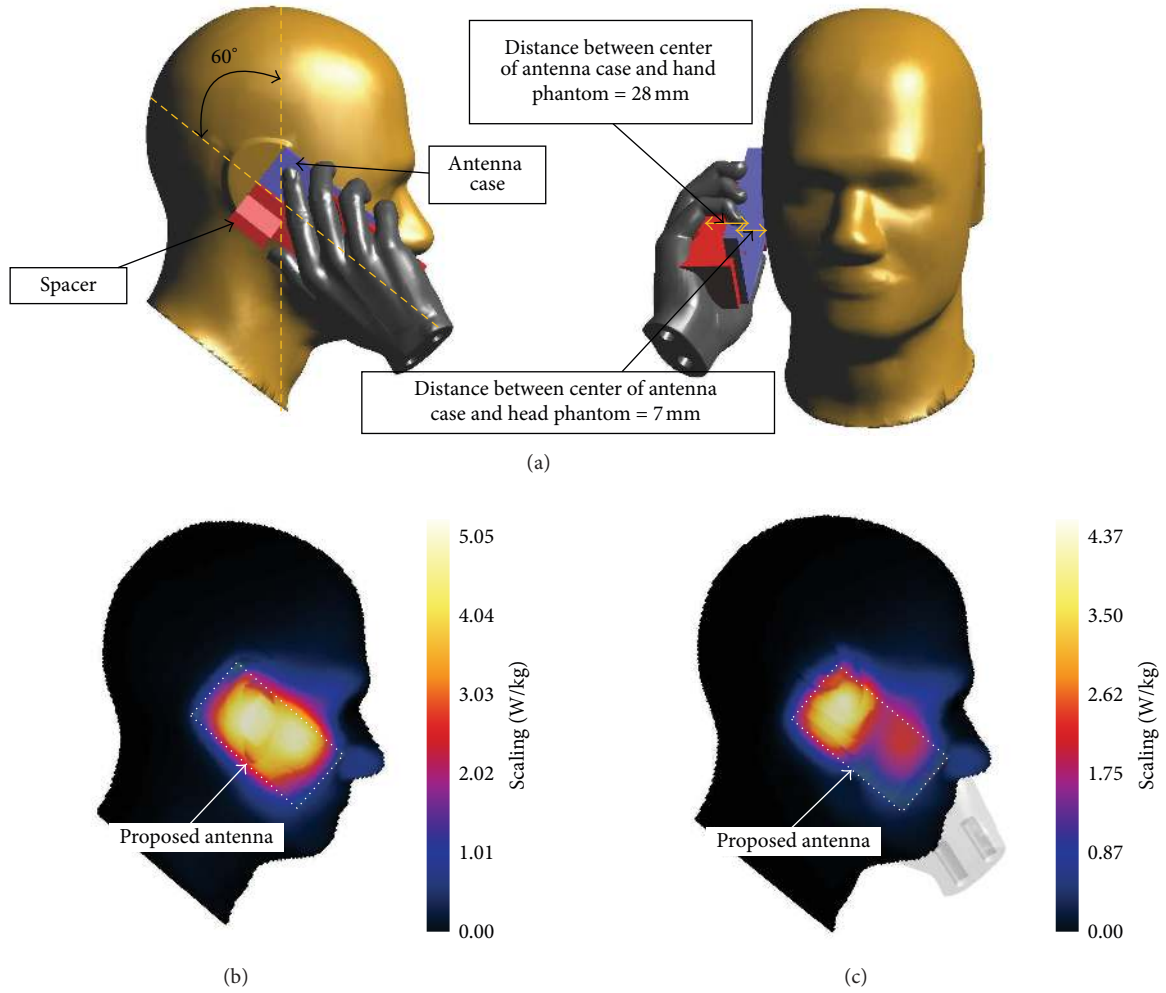
FIGURE 12: SAR simulation models. (a) Simulation setup. (b) SAR distribution in the head phantom at 1795 MHz. (c) SAR distribution in the head and hand phantoms at 1795 MHz.

efficiency at the low band is lower than that at the high band owing to the coupling between the ground plane and branch line. The measured gain varies from −0.91 to 0.25 dBi at the low band and from 1.4 to 5.48 dBi at the high band.

To evaluate the specific absorption rate (SAR) of the proposed antenna, a SAR simulation model that includes head and hand phantoms supported by SEMCAD is used [12]. The relative permittivity and conductivity of the phantom used in the simulation are listed in Table 1.

Figure 12(a) shows the simulation setup for the antenna with phantoms. The antenna, including the casing, is held by the hand phantom and attached to the head phantom. The distance between the center of the antenna case and hand phantom is 28 mm, and that between the center of the antenna case and head phantom is 7 mm. These simulation setups are based on the method used in [13]. Figures 12(b) and 12(c) show the SAR distributions at 1795 MHz where the SAR value is maximum. These distributions indicate that the maximum points of the SAR are located beneath the ear position.

The simulated results for the return loss, SAR values, and desired input power, which do not exceed the SAR limit (1.6 W/kg), are listed in Table 2. Because the proposed antenna covers the hepta-band, the simulated frequencies are chosen to be the center frequency of each desired band. When the input power is 1 W, the maximum SAR values are 5.05 W/kg for the head only and 4.37 W/kg for the head and hand at 1795 MHz. The American National Standards Institute requires that the SAR value should be below 1.6 W/kg over a volume of 1 g of tissue [14]. To satisfy the SAR limitation, the input power should be below 0.31 W.

The simulated antenna gain and efficiency with the head and hand phantoms are listed in Table 3. The antenna efficiency and gain with head and hand phantoms are reduced substantially since the antenna placed at the bottom side of a terminal is wrapped around by the hand.

Figure 13 shows the measured SAR distribution for the fabricated antenna on the head phantom. The SPEAG dosimetric assessment system (DASY-4) was used to perform SAR measurements [15]. The 1 g and 10 g SAR values when the
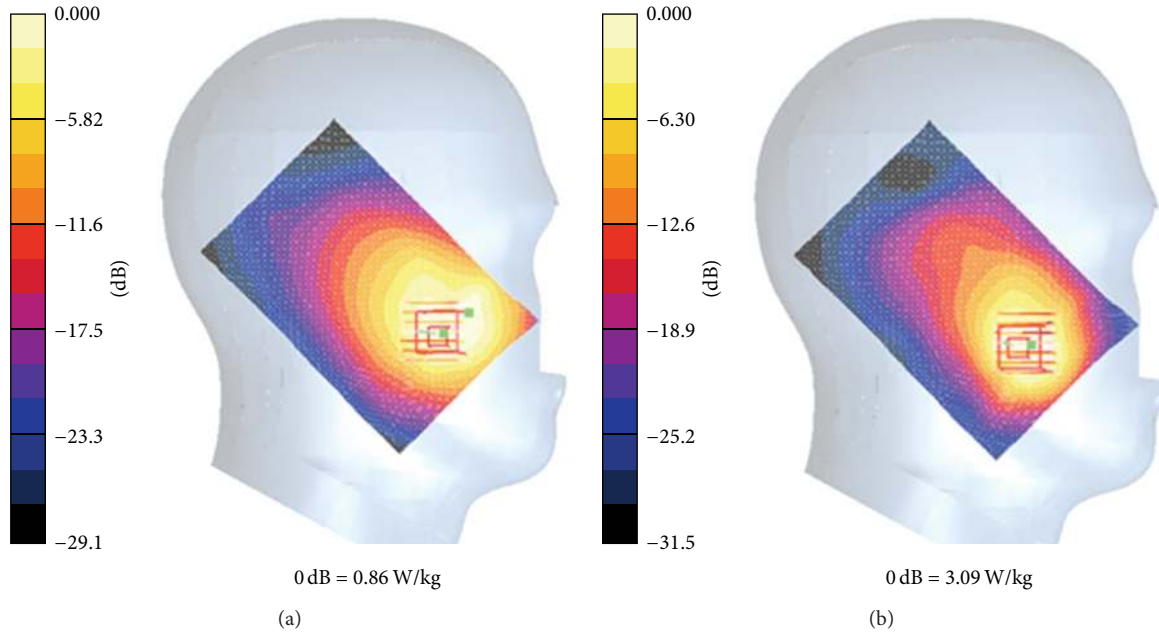
FIGURE 13: Measured SAR distributions in the head phantom (a) at 840 MHz and (b) at 1850 MHz (input power: 0.1 W).

TABLE 1: Relative permittivity and conductivity in the simulation.

Frequency (MHz)	Head		Hand	
	Relative permittivity	Conductivity	Relative permittivity	Conductivity
859	41.5	0.9	30.3	0.59
920	41.5	0.97	30	0.62
1795	40	1.4	27	0.99
1920	40	1.4	26.7	1.04
2045	40	1.4	26.5	1.09
2352.5	39.2	1.8	25.7	1.32
2595	39.2	1.8	25.7	1.32

TABLE 2: Simulated results of the return loss and SAR for the proposed antenna with the head and hand models.

Frequency (MHz)	Head only			Head and hand		
	Return Loss (dB)	1-g SAR (W/kg)	Input power for limit [14] (W)	Return Loss (dB)	1-g SAR (W/kg)	Input power for limit [14] (W)
859	14.94	3.84	0.41	6.43	2.27	0.70
920	6.78	4.59	0.34	6.74	3.06	0.52
1795	13.8	5.05	0.31	9.55	4.37	0.36
1920	8.75	4.34	0.36	7.19	3.74	0.42
2045	6.63	4.26	0.37	6.36	3.32	0.48
2352.5	4.36	3.74	0.42	4.49	2.17	0.73
2595	12.24	2.97	0.53	8.13	1.11	1.44

input power is 0.1 W and input powers that should not exceed the SAR limit [14] are listed in Table 4. The measured SAR values are greater than simulated ones, because the antenna is attached to the phantom without a case in the measurement setup.

5. Conclusion

A multiband antenna for the LTE/GSM/UMTS band operation has been proposed in this paper. The proposed antenna, which consists of the MPIFA and folded-loop antenna, has

TABLE 3: Simulated gain and efficiency for the proposed antenna with the head and hand phantoms.

Frequency (MHz)	Head only		Head and hand	
	Gain (dBi)	Efficiency (%)	Gain (dBi)	Efficiency (%)
859	−3.34	17.03	−8.06	7.02
920	−3.10	12.72	−7.06	7.49
1795	3.81	49.14	0.98	21.52
1920	3.96	46.14	1.62	21.13
2045	4.06	42.60	1.77	20.09
2352.5	4.19	35.58	0.58	14.20
2595	2.33	50.17	0.97	22.33

TABLE 4: Measured 1-g and 10-g SAR values for the fabricated antenna with head phantom (input power: 0.1 W).

Frequency (MHz)	Head phantom		
	1-g SAR (W/kg)	10-g SAR (W/kg)	Input power for limit [14] (W)
840	0.79	0.44	0.202
935	1.00	0.64	0.160
1850	2.79	1.51	0.057
2450	2.03	0.99	0.078

four resonant frequencies. The antenna provides wide 6 dB return loss bandwidth at both the low and high bands. The measured results of the fabricated antenna agree well with the simulated results. The measured radiation patterns are almost omnidirectional, and the measured efficiency is suitable for the desired LTE/GSM/UMTS band.

Conflict of Interests

The authors declare that there is no conflict of interests regarding the publication of this paper.

Acknowledgments
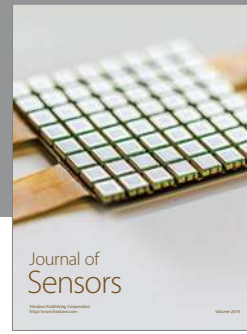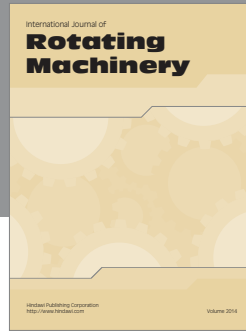
References

[1] A. Ghosh, R. Ratasuk, B. Mondal, N. Mangalvedhe, and T. Thomas, "LTE-advanced: next-generation wireless broadband technology," *IEEE Wireless Communications*, vol. 17, no. 3, pp. 10–22, 2010.

[2] C. Lee and K. Wong, "Planar monopole with a coupling feed and an inductive shorting strip for LTE/GSM/UMTS operation in the mobile phone," *IEEE Transactions on Antennas and Propagation*, vol. 58, no. 7, pp. 2479–2483, 2010.

[3] K. C. Lin, C. H. Lin, and Y. C. Lin, "Simple printed multiband antenna with novel parasitic-element design for multistandard mobile phone applications," *IEEE Transactions on Antennas and Propagation*, vol. 61, no. 1, pp. 488–491, 2013.

[4] J. Anguera, A. Andujar, and C. Garcia, "Multiband and small coplanar antenna system for wireless handheld devices," *IEEE Transactions on Antennas and Propagation*, vol. 61, no. 7, pp. 3782–3789, 2013.

[5] K. L. Wong, W. Y. Chen, and T. W. Kang, "On-board printed coupled-fed loop antenna in close proximity to the surrounding ground plane for penta-band WWAN mobile phone," *IEEE Transactions on Antennas and Propagation*, vol. 59, no. 3, pp. 751–757, 2011.

[6] X. Zhao, K. Kwon, and J. Choi, "MIMO antenna using resonance of ground planes for 4G mobile application," *The Journal of Korea Electromagnetic Engineering Society*, vol. 13, no. 1, pp. 51–53, 2013.

[7] Y. L. Ban, J. H. Chen, J. L. W. Li, and Y. Wu, "Small-size printed coupled-fed antenna for eight-band LTE/GSM/UMTS wireless wide area network operation in an internal mobile handset," *IET Microwaves, Antennas & Propagation*, vol. 7, no. 6, pp. 399–407, 2013.

[8] K. L. Wong, M. F. Tu, C. Y. Wu, and W. Y. Li, "On-board 7-band WWAN/LTE antenna with small size and compact integration with nearby ground plane in the mobile phone," *Microwave and Optical Technology Letters*, vol. 52, no. 12, pp. 2847–2853, 2010.

[9] J. Guo, L. Zhou, B. Sun, and Y. Zou, "Magneto-electric monopole antenna for terminal multiband applications," *Electronics Letters*, vol. 48, no. 20, pp. 1249–1250, 2012.

[10] S. Jeon, Y. Liu, S. Ju, and H. Kim, "PIFA with parallel resonance feed structure for wideband operation," *Electronics Letters*, vol. 47, no. 23, pp. 1263–1265, 2011.

[11] "HFSS: High Frequency Structure Simulator," v. 14.0.0, ANSYS Corp., 2013.

[12] X. Semcad, "A FDTD-Based Electromagnetic Simulator," version 14.8 Bernina, Schmid & Partner Engineering AG, Zurich, Switzerland, 2013.

[13] CTIA, "CTIA certification test plan for mobile station over the air performance," in *Method of Measurement for Radiated RF Power and Receiver Performance*, 2011.

[14] IEEE, "IEEE Standard for safety levels with respect to human exposure to radio frequency electromagnetic fields, 3 kHz to 300 GHz," IEEE Standard C95.1-1999, 1999.

[15] Schmid & Partner Engineering, AG, http://www.speag.com/speag.